PTEP

Prog. Theor. Exp. Phys. **2022** 033B09(17 pages)
DOI: 10.1093/ptep/ptac022

The magic square and half-hypermultiplets in F-theory

Rinto Kuramochi[1], Shun'ya Mizoguchi[1,2,⋆], and Taro Tani[3]

[1]*Graduate University for Advanced Studies (Sokendai), Tsukuba, Ibaraki, 305-0801, Japan*
[2]*Theory Center, Institute of Particle and Nuclear Studies, KEK, Tsukuba, Ibaraki, 305-0801, Japan*
[3]*National Institute of Technology, Kurume College, Kurume, Fukuoka, 830-8555, Japan*
⋆E-mail: mizoguch@post.kek.jp

Received August 25, 2021; Revised December 27, 2021; Accepted February 21, 2022; Published February 23, 2022

In six-dimensional F-theory/heterotic string theory, half-hypermultiplets arise only when they correspond to particular quaternionic Kähler symmetric spaces, which are mostly associated with the Freudenthal–Tits magic square. Motivated by the intriguing singularity structure previously found in such F-theory models with a gauge group $SU(6)$, $SO(12)$, or E_7, we investigate, as the final magical example, an F-theory on an elliptic fibration over a Hirzebruch surface of the non-split I_6 type, in which the unbroken gauge symmetry is supposed to be $Sp(3)$. We find significant qualitative differences between the previous F-theory models associated with the magic square and the present case. We argue that the relevant half-hypermultiplets arise at the E_6 points, where half-hypermultiplets **20** of $SU(6)$ would have appeared in the split model. We also consider the problem on the non-local matter generation near the D_6 point. After stating what the problem is, we explain why this is so by using the recent result that a split/non-split transition can be regarded as a conifold transition.

Subject Index B29, B80

1. Introduction

F-theory [1–3] is a framework of nonperturbative compactifications of type IIB string theory containing general (p, q)-7-branes. The nonperturbativeness of F-theory arises due to the nonlocality among the 7-branes and the strings, where the $SL(2, \mathbb{Z})$ identification before and after a move of a string among 7-branes gives rise to open-string-like light pronged objects, string junctions. In the dual M-theory picture, they correspond to wrapped M2-branes around vanishing cycles. These objects account for the emergence of the exceptional gauge symmetry and matter in the spinor representation in a type II setup, which is one of the virtues of F-theory in the application to the phenomenological model building.

In F-theory, matter typically arises at the intersections of 7-branes, where the singularity of the gauge brane with gauge group H is "enhanced" to that labeled by some another higher-rank group G [2–6].[1] In generic cases, G is one rank higher than H, and in six dimensions the matter arising at the intersection is in most cases a hypermultiplet transforming as $G/(H \times U(1))$, which

[1]The matter localization at the intersection of the spectral cover C and the zero section σ_{B_2} (in the four-dimensional case) was originally shown in Refs. [7,8] by using the Leray spectral sequence. It is precisely where the singularity gets enhanced on B_2, though of course the spectral cover C cannot be regarded as the matter 7-brane itself as it intersects with the elliptic fiber. This coincidence was explained in Refs. [9,10] in terms of the Mordell–Weil lattice of a rational elliptic surface [11].

© The Author(s) 2022. Published by Oxford University Press on behalf of the Physical Society of Japan.
This is an Open Access article distributed under the terms of the Creative Commons Attribution License (https://creativecommons.org/licenses/by/4.0/), which permits unrestricted reuse, distribution, and reproduction in any medium, provided the original work is properly cited.
Funded by SCOAP[3]

Downloaded from https://academic.oup.com/ptep/article/2022/3/033B09/6534943 by DESY-Zentralbibliothek user on 25 April 2022

Table 1. The Freudenthal–Tits magic square for $\mathbb{A}$, $\mathbb{B}$ being either of the four division algebras $\mathbb{R}$, $\mathbb{C}$, $\mathbb{H}$, $\mathbb{O}$. They are all compact Lie algebras with definite signatures. If the division algebras are replaced by split composition algebras, the entries become different real forms with the same complexifications.

$\mathbb{B}\backslash\mathbb{A}$	$\mathbb{R}$	$\mathbb{C}$	$\mathbb{H}$	$\mathbb{O}$
$\mathbb{R}$	$\mathfrak{so}(3)$	$\mathfrak{su}(3)$	$\mathfrak{sp}(3)$	$\mathfrak{f}_4$
$\mathbb{C}$	$\mathfrak{su}(3)$	$\mathfrak{su}(3) \oplus \mathfrak{su}(3)$	$\mathfrak{su}(6)$	$\mathfrak{e}_6$
$\mathbb{H}$	$\mathfrak{sp}(3)$	$\mathfrak{su}(6)$	$\mathfrak{so}(12)$	$\mathfrak{e}_7$
$\mathbb{O}$	$\mathfrak{f}_4$	$\mathfrak{e}_6$	$\mathfrak{e}_7$	$\mathfrak{e}_8$

determines a homogeneous Kähler manifold. However, in some cases matter emerging at the intersection is not a full hypermultiplet but a *half*-hypermultiplet. For example [4], when (G, H) are $(E_6, SU(6))$, $(E_7, SO(12))$, or (E_8, E_7), half-hypermultiplets appear in **20**, **32**, or **56** of the respective H. They are all pseudo-real representations and correspond, not to homogeneous Kähler manifolds, but to quaternionic Kähler symmetric spaces known as Wolf spaces [12–15] (see Ref. [16] for a review):

$$\frac{E_6}{SU(6) \times SU(2)}, \qquad \frac{E_7}{SO(12) \times SU(2)}, \qquad \frac{E_8}{E_7 \times SU(2)}. \tag{1}$$

In Ref. [17], an explicit resolution of the codimension-two singularity was carried out for the first example $(G, H) = (E_6, SU(6))$. It was found that the codimension-two singularity was already resolved by blowing up the nearby codimension-one $A_5 = SU(6)$ singularities without any additional blow-up at that point, although the Kodaira fiber type right over the intersection point was IV^*, which would mean an E_6 singularity. The number of exceptional curves over the codimension-two point is the same as that of the codimension-one loci supporting a fiber of the type I_6. It was also found that the intersection diagram at the codimension-two point was different from that of the nearby codimension-one loci, explaining the generation of the half-hypermultiplet at that point. This type of resolution was called an *incomplete resolution* [17]. In Ref. [18], a similar analysis was performed for $(G, H) = (E_7, SO(12))$ and (E_8, E_7) to find similar features.

We should note that all these enhancements are relevant in the applications to F-theory grand unified theory (GUT) model building. For instance, the enhancement $SU(6) \to E_6$ is the one at the (codimension-three) Yukawa Kähler point on the $\bar{\mathbf{5}}$ matter curve in the four-dimensional $SU(5)$ F-GUT model. Similarly, the enhancements $SO(12) \to E_7$ and $E_7 \to E_8$ are the ones at the Yukawa points on the $\overline{\mathbf{10}}$ and **27** curves in the $SO(10)$ and E_6 F-GUT models, respectively. Also, the multiple (= higher-rank) enhancement $SU(5) \to E_7$ (or E_8), which includes these special enhancements as intermediate steps, is relevant to the F-theory family unification scenario [19] aiming to implement the supersymmetric E_7 coset sigma model [20] in F-theory.

Incidentally, the three symmetric spaces in Eq. (1) are precisely the ones obtained by taking a quotient of the groups of the entries of the Freudenthal–Tits magic square (Table 1). The relation between quaternionic Kähler manifolds and the magic square was noticed some time ago in Ref. [16]. Indeed, the Gs and Hs comprising the symmetric spaces in Eq. (1) are the groups of the Lie algebras listed in the bottom and the second bottom rows of the rightmost three columns in the table. Motivated by this observation, in this paper we focus on the final remaining column of the magic square and study the corresponding six-dimensional F-theory compactification on an elliptic CY3 over a Hirzebruch surface [2,3]. We can indeed find in

Downloaded from https://academic.oup.com/ptep/article/2022/3/033B09/6534943 by DESY-Zentralbibliothek user on 25 April 2022

Ref. [4] a model with the gauge group $C_3 = Sp(3)$ yielding half-hypermultiplets in $F_4/(Sp(3) \times SU(2)) = \mathbf{14}'$ as a part of the massless matter: the *non-split* I_6 model.

One of our interests is what kind of singularity gives rise to the supermultiplet of chiral matter in this representation. The equation defining the non-split I_6 model is obtained by modifying that of the split I_6 model [4]. The latter gives the $SU(6)$ unbroken gauge symmetry with matter fields in **20**, **15**, and **6**, where the singularity is enhanced from A_5 to E_6, D_6, and A_6 respectively. A **20** is a half-hypermultiplet in the split case studied in Ref. [17]. We can obtain the equation for the non-split I_6 model by a certain change of the sections that characterize the equation of the split I_6 model. With this change, the local structures of the singularities at the E_6 and A_6 points remain intact, but only those at the D_6 points are affected, so we examine the singularity structure at the D_6 points in the non-split I_6 model.

The non-split models are known to have some puzzles regarding the generation of matter fields [4,21–25]. The equation defining the non-split I_6 model is obtained by replacing the square of a particular section h^2_{n+2-r} (see text for the definition) in the split I_6 equation with a non-square section $h_{2n+4-2r}$. This global non-factorization implies monodromy among the exceptional fibers, which is interpreted as a feature that causes the gauge group to reduce from the simply-laced $SU(6)$ to the non-simply-laced $Sp(3)$ [4]. However, there is a puzzle here: At each double zero locus of h_{n+2-r} there appears a hypermultiplet in **15** of $SU(6)$ in the split model. Therefore, the anomaly cancellation requires that the hypermultiplets in **15** of $SU(6)$ at the double zeros should *split in pairs* according to the replacement of the section, but the **14** (not $\mathbf{14}'$, see below) of $Sp(3)$, supposed to arise from the **15** of $SU(6)$, is a *real* (not a *pseudo-real*) representation, which does not allow half-hypermultiplets. This is the first puzzle.

There is another curious feature about this non-split model: As in Refs. [17,18], we consider a local equation which exhibits the singularity structure near a single zero locus of the section $h_{2n+4-2r}$. The resolution of the singularity turns out to be an "incomplete" resolution, meaning that the codimension-two "D_6" singularity is already resolved when the resolution of the codimension-one singularity is completed. However, the difference from the previous three magical examples is that the intersection matrix of the exceptional curves at the codimension-two[2] D_6 point remains identical to that at a nearby point on the codimension-one singularity. Therefore, the configuration of the exceptional curves generated there does not indicate that any chiral matter field is localized there.

Note that this "non-locality," which has been a problem since Ref. [4], is different from that associated with the mirror images produced by the orientifold fixed plane. Indeed, since the singularity is apparently enhanced from A_5 to D_6 at a zero locus of $h_{2n+4-2r}$, it can be seen as the point where the D-branes intersect with an orientifold fixed plane [26]. However, the "non-locality" that arises there is around each $h_{2n+4-2r}$ locus, which is different from the non-locality of matter in question that should arise across each pair of $h_{2n+4-2r}$ loci.

Therefore, these puzzles require a new understanding of charged matter generation in the non-split model, other than wrapped branes around vanishing cycles [5] or string junctions ending on the intersections of 7-branes [6]. Very recently, it was shown [27] that the split/non-split transition in F-theory can be regarded as, apart from some exceptional cases, a conifold transition associated with the relevant conifold singularities. In this paper we will use this fact to discuss how the necessary matter can emerge from the geometry of the non-split model.

[2]Note that this codimension is counted in the base space of the elliptic fibration, and not in the total space of the Calabi–Yau.

Downloaded from https://academic.oup.com/ptep/article/2022/3/033B09/6534943 by DESY-Zentralbibliothek user on 25 April 2022

More precisely, since the non-split model corresponds to the "deformed side" of the conifold transition, there arise three-cycles instead of two-cycles on the "resolved side," which is the split model. We will discuss what branes can give a chiral matter field with the three-cycles.

On the other hand, as for the question of where the **14**′s are generated, we argue that they just arise as the $Sp(3)$ decomposition of the **20**s of $SU(6)$ at the E_6 points, and not at the D_6 points.

The organization of this paper is as follows: In Sect. 2 we give a brief review of the Freudenthal–Tits magic square and point out its relation to half-hypermultiplets in F-theory. In Sect. 3 we consider the global split and non-split I_6 models and examine their matter spectra. In Sect. 4, we perform a concrete blowing-up process of the "D_6" singularity of the non-split I_6 local equation. In Sect. 5 we introduce the recent result of Ref. [27] and show how it is used to resolve the issue of non-local matter. The final section is devoted to conclusions.

2. The magic square and half-hypermultiplets in F-theory

2.1 *The Freudenthal–Tits magic square*

A Freudenthal–Tits magic square is a four-by-four table whose entries are Lie algebras. They are determined by specifying a pair of composition algebras $(\mathbb{A}, \mathbb{B})$. When these composition algebras are the ones over the real number field $\mathbb{R}$, they are either one of the four division algebras $\mathbb{R}$, $\mathbb{C}$, $\mathbb{H}$, and $\mathbb{O}$, or they are one of the "split" algebras of $\mathbb{C}$, $\mathbb{H}$, and $\mathbb{O}$, which are non-compact analogues of the corresponding division algebras. In this case, each entry of the magic square is some real form of a complex Lie algebra.

If $(\mathbb{A}, \mathbb{B})$ are a pair of either of the four division algebras $\mathbb{R}$, $\mathbb{C}$, $\mathbb{H}$, and $\mathbb{O}$, the magic square consists of compact Lie algebras with definite signatures (Table 1), while if $(\mathbb{A}, \mathbb{B})$ are chosen from the set of $\mathbb{R}$ and the three split algebras, the entries are all split real forms of the same complexifications as those of the compact Lie algebras in the corresponding cells. They typically arise (apart from a few exceptions) as (Lie algebras of) duality groups or hidden symmetries of dimensionally reduced maximally symmetric supergravities, bosonic string or the NS–NS sector effective theory, and pure gravities. Finally, if $\mathbb{A}$ is a division algebra and $\mathbb{B}$ is a split algebra, the magic square conprises a special set of real forms of exceptional Lie algebras arising as scalar manifolds of dimensional reductions of $D = 5$ "magical" supergravities [28–31].

The $(\mathbb{A}, \mathbb{B})$ entry of the magic square always has the following structure:

$$\mathfrak{der}\,\mathbb{A} \oplus \mathfrak{der}\,\mathfrak{J}^{\mathbb{B}} \oplus \left(\mathbb{A}_0 \otimes \mathfrak{J}_0^{\mathbb{B}}\right), \tag{2}$$

where $\mathfrak{der}\,\mathbb{A}$ and $\mathfrak{der}\,\mathfrak{J}^{\mathbb{B}}$ are the Lie algebras of the automorphism groups of $\mathbb{A}$ and $\mathfrak{J}^{\mathbb{B}}$, respectively, where $\mathfrak{J}^{\mathbb{B}}$ is the Jordan algebra associated with the composition algebra $\mathbb{B}$. $\mathbb{A}_0$ and $\mathfrak{J}_0^{\mathbb{B}}$ denote their traceless parts.

For example, for the compact case $\mathbb{A}, \mathbb{B} = \mathbb{R}, \mathbb{C}, \mathbb{H}, \mathbb{O}$ (Table 1),[3]

$$\mathfrak{der}\,\mathbb{A} = 0, 0, \mathfrak{su}(2), \mathfrak{g}_2, \tag{3}$$

$$\mathfrak{der}\,\mathfrak{J}^{\mathbb{B}} = \mathfrak{so}(3), \mathfrak{su}(3), \mathfrak{sp}(3), \mathfrak{f}_4, \tag{4}$$

$$\mathbb{A}_0 = 0, 0, \mathbf{3}, \mathbf{7} \quad \text{of } \mathfrak{der}\,\mathbb{A}, \tag{5}$$

[3] In this paper we use the notations $\mathfrak{sp}(n)$ and $Sp(n)$ to denote the Lie algebra and the Lie group of the C_n-type Dynkin diagram.

Downloaded from https://academic.oup.com/ptep/article/2022/3/033B09/6534943 by DESY-Zentralbibliothek user on 25 April 2022

$$\mathfrak{J}_0^{\mathbb{B}} = \mathbf{5}, \mathbf{8}, \mathbf{14}, \mathbf{26} \quad \text{of } \mathfrak{der}\,\mathfrak{J}^{\mathbb{B}}. \tag{6}$$

Then, for instance, $\mathfrak{e}_7$ allows a decomposition

$$E_7 \supset SU(2) \times F_4,$$
$$\mathbf{133} = (\mathbf{3}, \mathbf{1}) \oplus (\mathbf{1}, \mathbf{52}) \oplus (\mathbf{3}, \mathbf{26}) \tag{7}$$

for $\mathbb{A} = \mathbb{H}$, $\mathbb{B} = \mathbb{O}$, and also

$$E_7 \supset G_2 \times Sp(3),$$
$$\mathbf{133} = (\mathbf{14}, \mathbf{1}) \oplus (\mathbf{1}, \mathbf{21}) \oplus (\mathbf{7}, \mathbf{14}) \tag{8}$$

for $\mathbb{A} = \mathbb{O}$, $\mathbb{B} = \mathbb{H}$. The other Lie algebras allow similar decompositions.

Remark 1. In this paper the word "split" is used in three different meanings:

1. A "split" composition algebra, which is a non-compact version of $\mathbb{C}$, $\mathbb{H}$, or $\mathbb{O}$ with an indefinite bilinear form.
2. A "split" real form of a complex Lie algebra, which has, besides the Cartan subalgebra, an equal number of positive and negative generators with respect to the invariant bilinear form.
3. Finally, the word "split" appears in the classification of singularities or the fiber types of exceptional curves [4]. Singularities of the "split" type are the ones in which relevant exceptional curves factor globally so that they yield simply-laced gauge symmetries.

The first two are closely related in that split real forms of item 2 arise in the magic square when the composition algebras are taken to be split ones in the sense of item 1. The third one is, however, a different notion from the other two.

2.2 *Half-hypermultiplets in F-theory*

In Ref. [4], a detailed analysis was carried out on the matter spectra of six-dimensional F-theory compactifications on an elliptically fibered Calabi–Yau threefold over a Hirzebruch surface [2,3] for various patterns of unbroken gauge groups. In particular, it was revealed that there were (essentially) four cases of unbroken gauge groups[4] in which *half-hypermultiplets* (rather than normal hypermultiplets) appeared as massless matter. They are listed in Tables 2 and 3. These spectra can be confirmed either by the heterotic index calculation [32][5] or by the generalized Green–Schwarz mechanism using the divisor data of the Hirzebruch surface [9,34].[6] They satisfy the anomaly-free constraint for one of the E_8 factors with instanton number $12 + n$ [4],

$$n_H - n_V = 30n + 112. \tag{9}$$

[4]There is, in fact, one more example in Ref. [4] where half-hypermultiplets arise as massless matter: the **32** of $SO(11)$. This is also a non-split model (I_2^{*ns}), and this **32** is easily seen to arise at the E_7 point, where the corresponding split model (I_2^{*s}) with the $SO(12)$ gauge symmetry also yields **32**.

[5]For $Sp(3)$, the dual heterotic gauge bundle is $SU(2) \times G_2$ since the maximal embedding is $E_8 \supset SU(2) \times G_2 \times Sp(3)$ (see, e.g., Ref. [33] for the branching rules). The spectrum in Table 3 is obtained by distributing the $12 + n$ instantons as $(4 + r, 8 + n - r)$ in $(SU(2), G_2)$.

[6]For $Sp(3)$, the relevant indices of a representation **R** for examining the generalized Green–Schwarz mechanism are given by (index(**R**), $x_{\mathbf{R}}$, $y_{\mathbf{R}}$) = (8, 14, 3), (1,1,0), (4, −2, 3), and (5, −7, 6) for **R** = **Adj**, **6**, **14**, and **14**′, respectively, where $\mathrm{tr}_{\mathbf{R}} F^2 = \mathrm{index}(\mathbf{R})\mathrm{tr}_{\mathbf{6}} F^2$ and $\mathrm{tr}_{\mathbf{R}} F^4 = x_{\mathbf{R}} \mathrm{tr}_{\mathbf{6}} F^4 + y_{\mathbf{R}} (\mathrm{tr}_{\mathbf{6}} F^2)^2$. By using these data and assuming that the charged matter spectrum only contains **6**, **14**, and **14**′, one can solve the equations of the generalized Green–Schwarz mechanism on F_n and obtain the unique solution given in Table 3.

Downloaded from https://academic.oup.com/ptep/article/2022/3/033B09/6534943 by DESY-Zentralbibliothek user on 25 April 2022

Table 2. Three cases in which half-hypermultiplets appear as massless matter in six-dimensional F-theory on an elliptic CY3 over $\mathbb{F}_n$ / heterotic string theory on K3 (quoted from [4, Table 3]).

Gauge group H	Fiber type	Enhancement G	Matter representation	Multiplicity	Homogeneous space
E_7	III^{*s}	E_8	$\frac{1}{2}\mathbf{56}$	$n+8$	$\frac{E_8}{E_7\times SU(2)}$
			$\mathbf{1}$	$2n+21$	—
D_6	I_2^{*s}	E_7	$\frac{1}{2}\mathbf{32}$	$n+4$	$\frac{E_7}{SO(12)\times SU(2)}$
		D_7	$\mathbf{12}$	$n+8$	$\frac{SO(14)}{SO(12)\times U(1)}$
			$\mathbf{1}$	$2n+18$	—
A_5	I_6^s	E_6	$\frac{1}{2}\mathbf{20}$	r	$\frac{E_6}{SU(6)\times SU(2)}$
		D_6	$\mathbf{15}$	$n+2-r$	$\frac{SO(12)}{SU(6)\times U(1)}$
		A_6	$\mathbf{6}$	$2n+16+r$	$\frac{SU(7)}{SU(6)\times U(1)}$
			$\mathbf{1}$	$3n+21-r$	—

Table 3. The massless matter spectrum of six-dimensional heterotic string theory on K3 with an unbroken $Sp(3)$ gauge symmetry. This is anomaly free, and also contains half-hypermultiplets.

Gauge group	Representation	Multiplicity
C_3	$\frac{1}{2}(\mathbf{14'}+\mathbf{6})$	r
	$\mathbf{14}$	$n+1-r$
	$\mathbf{6}$	$2n+16+r$
	$\mathbf{1}$	$4n+23-2r$

As we can see, the representations **56**, **32**, and **20**, together with **14**$'$ and **6**, to which the half-hypermultiplets belong, are precisely those of quaternionic Kähler manifolds (or "Wolf spaces"). All but the last **6** are obtained by taking the Lie groups of the extreme bottom and the third rows of the magic square as the groups of the numerator and denominator of the homogeneous space. The denominator groups also always come with an $SU(2)$ factor in contrast to the case of ordinary hypermultiplets, where the denominator group contains not an $SU(2)$ but a $U(1)$ factor. In the latter case, the symmetric space is a homogeneous Kähler manifold [19]. In the M-theory Coulomb branch analysis of codimension-two or higher singularities [35], the Weyl group invariant phases of this $SU(2)$ were shown to correspond to the resolutions yielding half-hypermultiplets.

Let us summarize what is known so far, for the three simply-laced split examples of Table 2, about the resolutions of the codimension-two singularities that yield half-hypermultiplets. The resolutions of the third example were studied in Ref. [17], and the those of the first and second ones were worked out in Ref. [18]. The main relevant features are:[7]

(i) As in Refs. [2,3], let z (z') be the affine coordinate of the $\mathbb{P}^1$ fiber ($\mathbb{P}^1$ base) of the Hirzebruch surface $\mathbb{F}_n$. Suppose that we have a codimension-one singularity along the line $z=0$ with the fiber type specified in the second column of Table 2. Non-singlet matter arises where the singularity is "enhanced" from H to G, in the sense that the Kodaira fibers read off at *right over that point* have intersections specified by the Dynkin diagram of G. How-

[7] The local coordinate s parametrizing the base P^1 of F_n will be denoted by w in Sect. 4 when we blow up the singularities.

Downloaded from https://academic.oup.com/ptep/article/2022/3/033B09/6534943 by DESY-Zentralbibliothek user on 25 April 2022

ever, where the half-hypermultiplets appear, the codimension-two singularity is already resolved by blowing up the nearby codimension-one singularities. No additional blow-up at the codimension-two point is required, even though the singularity is "enhanced" there in the sense explained above. Such type of resolution is called an *incomplete resolution* [17].

(ii) In an incomplete resolution, the relevant section that vanishes at codimension two goes like $O(s)$, where s is a local coordinate holomorphic in z', and $s = 0$ is the codimension-two singularity. In this case, although the number of blow-ups required to resolve it is the same as that to resolve the nearby generic codimension-one singularities, the intersection matrix of the exceptional curves at $s = 0$ is not the same as the generic one determined by the Cartan matrix of H (nor that of G), but turns out to be a curious non-Dynkin diagram with some nodes having self-intersections $-\frac{3}{2}$.

(iii) In the first three examples of Table 2 studied in Refs. [17,18], $\frac{3}{2}$ is the length square of the weight vector of the representations to which the half-hypermultiplets belong. It was confirmed that although the intersection matrix was not the (minus of the) Cartan matrix of G, the exceptional curves at $s = 0$ formed an extremal ray that could span all the weights of the relevant pseudo-real representation of the half-hypermultiplets.

(iv) In the first two examples, several codimension-one singularities arise during the intermediate stages of the blow-up process, and there are several options in which singularity we blow up first, and which we do afterwards. Depending on the ordering of the blow-ups, one obtains different intersection diagrams of the exceptional curves at the codimension-two point $s = 0$ [18]. More specifically, the intersection diagram on every other row found in Ref. [35] can be obtained in this way, but not all of them.

(v) Instead, when the relevant section vanishes like $O(s^2)$ at the codimension-two point, the singularity becomes stronger than the case above so that an additional conifold singularity arises. A small resolution generates an extra exceptional fiber at that point so that it completes the proper Dynkin diagram of group G. This type of resolution is called a *complete resolution* [17].

3. Six-dimensional $Sp(3)$ global model

3.1 *The non-split I_6 equation on F_n*

In this section we consider a six-dimensional F-theory compactification on an elliptic fibration over a Hirzebruch surface $\mathbb{F}_n$ in which the unbroken gauge symmetry reduces to $Sp(3)$. We work in the dP_9 fibration so that we focus on one of the two E_8s of the heterotic dual.

As was shown in Ref. [4], the equation of this curve is the one that supports an I_6 Kodaira fiber of the non-split type at $z = 0$. An I_6 non-split curve may be obtained by replacing the relevant factorized section of a split I_6 curve with a non-factorized one. More specifically, consider Tate's form of the equation describing the elliptic fibration:

$$-(y^2 + a_1xy + a_3y) + x^3 + a_2x^2 + a_4x + a_6 = 0. \tag{10}$$

As in Refs. [2,3], we use z and z' as the affine coordinates of the fiber and base P^1s of the Hirzebruch surface. $z = 0$ is the divisor of self-intersection $+n$. The equation for the theory

Downloaded from https://academic.oup.com/ptep/article/2022/3/033B09/6534943 by DESY-Zentralbibliothek user on 25 April 2022

with the unbroken group $H = SU(6)$ can be obtained by specializing the sections as

$$\begin{aligned} a_1 &= 2\sqrt{3}t_r h_{n-r+2}, \\ a_2 &= -3zt_r H_{n-r+4}, \\ a_3 &= 2\sqrt{3}z^2 u_{r+4} h_{n-r+2}, \\ a_4 &= z^3\left(t_r f_{n-r+8} - 3u_{r+4}H_{n-r+4}\right) + f_8 z^4, \\ a_6 &= z^5 u_{r+4} f_{n-r+8} + g_{12} z^6, \end{aligned} \tag{11}$$

where t_r, h_{n-r+2}, H_{n-r+4}, u_{r+4}, and f_{n-r+8} (together with f_8 and g_{12}) are the sections of appropriate line bundles over the base P^1 specified by their subscripts, which in this case denote nothing but the degrees of the polynomials in z'. It can be verified that Eq. (10) with Eq. (12) correctly reproduces the anomaly-free heterotic massless spectrum for an unbroken $SU(6)$ gauge group with $SU(3) \times SU(2)$ instanton numbers $(r, 12 + n - r)$ (see, e.g., Ref. [36]).

Remark 2. While Eqs. (10) and (12) successfully yield a consistent $SU(6)$ model, the vanising orders of $(a_1, a_2, a_3, a_4, a_6)$ in z are (0,1,2,3,5), which are the same as those for the split I_5 fiber type I_5^s and differ from the "standard" Tate's orders (0,1,3,3,6) for the split I_6 fiber type I_6^s classified in Ref. [4]. Indeed, it can be easily seen that the sections $(a_1, a_2, a_3, a_4, a_6)$ with orders (0,1,3,3,6) only result in the Weierstrass model of Eqs. (12)– (14) with constant t_r, that is, no instantons are distributed to the $SU(3)$ factor, and all the $12 + n$ instantons are in the $SU(2)$ factor. In fact, one can redefine y and x so that the vanishing orders of $(a_1, a_2, a_3, a_4, a_6)$ may become (0,1,3,3,6) only when $t_r \neq 0$, but cannot when $t_r = 0$ since the redefinitions of y and x contain shifts proportional to $\frac{1}{t_r}$, which diverge at $t_r = 0$.

By redefining y and x, we obtain the Weierstrass equation

$$0 = -y^2 + x^3 + f_{SU(6)}(z, z')x + g_{SU(6)}(z, z'), \tag{12}$$

$$\begin{aligned} f_{SU(6)}(z, z') \equiv & -3t_r^4 h_{n-r+2}^4 + 6zt_r^3 h_{n-r+2}^2 H_{n-r+4} \\ & + z^2\left(6t_r u_{r+4} h_{n-r+2}^2 - 3t_r^2 H_{n-r+4}^2\right) \\ & + z^3\left(t_r f_{n-r+8} - 3u_{r+4}H_{n-r+4}\right) + f_8 z^4, \end{aligned} \tag{13}$$

$$\begin{aligned} g_{SU(6)}(z, z') \equiv & \, 2t_r^6 h_{n-r+2}^6 - 6z\left(t_r^5 h_{n-r+2}^4 H_{n-r+4}\right) \\ & - 6z^2\left(t_r^3 u_{r+4} h_{n-r+2}^4 - t_r^4 h_{n-r+2}^2 H_{n-r+4}^2\right) \\ & + z^3\left(-t_r^3 f_{n-r+8} h_{n-r+2}^2 + 9t_r^2 u_{r+4} h_{n-r+2}^2 H_{n-r+4} - 2t_r^3 H_{n-r+4}^3\right) \\ & + z^4\left(-f_8 t_r^2 h_{n-r+2}^2 + t_r^2 f_{n-r+8} H_{n-r+4} + 3u_{r+4}^2 h_{n-r+2}^2 - 3t_r u_{r+4} H_{n-r+4}^2\right) \\ & + z^5\left(f_8 t_r H_{n-r+4} + u_{r+4} f_{n-r+8}\right) + g_{12} z^6, \end{aligned} \tag{14}$$

with a discriminant

$$4f_{SU(6)}^3 + 27g_{SU(6)}^2 = z^6 t_r^3 h_{n-r+2}^4 P_{2n+r+16} + z^7 t_r^2 h_{n-r+2}^2 Q_{3n+20} + z^8 R_{4n+24} + O(z^9), \tag{15}$$

where $P_{2n+r+16}$, Q_{3n+20}, and R_{4n+24} are some non-factorizable polynomials in z' of degrees specified by the subscripts. In generic cases, any two of t_r, h_{n-r+2}, and $P_{2n+r+16}$ do not share a common zero locus, which we assume in this paper. From Eqs. (13)– (15) we can see that the Kodaira fiber types over the zero loci of t_r, h_{n-r+2}, and $P_{2n+r+16}$ are respectively IV^*, I_2^*, and

Downloaded from https://academic.oup.com/ptep/article/2022/3/033B09/6534943 by DESY-Zentralbibliothek user on 25 April 2022

I_7, yielding the singularity enhancements from $H = SU(6)$ to $G = E_6$, D_6, and A_6 as presented in the third column of Table 2. We can also see that the h_{n-r+2} dependence of $f_{SU(6)}$ in Eq. (13) or $g_{SU(6)}$ in Eq. (14) is only through h^2_{n-r+2}, which allows us to replace every h^2_{n-r+2} in $f_{SU(6)}$ and $g_{SU(6)}$ with a generic polynomial $h_{2n-2r+4}$. The resulting equation is the one for I_6^{ns} [4].

3.2 *The massless spectrum*

As we will see explicitly in the next section, the replacement of the section $h^2_{n-r+2} \to h_{2n-2r+4}$ in the split I_6 equation results in the global non-factorization of the exceptional curves, which reduces the gauge group from $SU(6)$ to $Sp(3)$. Let us examine what matter multiplets are expected to arise in this model.

In the transition $I_6^s \leftrightarrow I_6^{ns}$, nothing changes in the local singularity structure near the zero loci of t_r and $P_{2n+r+16}$, where $\frac{1}{2}$**20** and **6** of $SU(6)$ appear as massless matter in the split theory; the string junctions or the vanishing cycles there do not "know" whether the total equation is of the split type or of the non-split type. The only change they feel is that of the gauge group, so they simply decompose into irreducible representations of $Sp(3)$, which is the gauge group of the non-split theory. Thus, at a zero locus of t_r, a half-hypermultiplet in **20** of $SU(6)$, of which the quaternionic Kähler manifold $E_6/(SU(6) \times SU(2))$ is comprised, is decomposed into half-hypermultiplets in **14**′ and **6** of $Sp(3)$, while at a zero of $P_{2n+r+16}$, a hypermultiplet in **6** of $SU(6)$ entirely becomes one in **6** of $Sp(3)$. Note that **6** is also a pseudo-real representation of $Sp(3)$, and the latter can be regarded as $2n + r + 16$ pairs of half-hypermultiplets. The **14**′ constitutes the quaternionic Kähler manifold $F_4/(Sp(3) \times SU(2))$, while the **6** does $Sp(4)/(Sp(3) \times SU(2))$. This will answer the original question of where the matter fields corresponding to the final magical coset arise: they arise at the E_6 points of the non-split I_6 model as an irreducible multiplet in the $Sp(3)$ decomposition of **20** of $SU(6)$.

3.3 *The puzzle of matter fields near the D_6 points*

On the other hand, there is a puzzle as we mentioned in Sect. 1: With the replacement $h^2_{n-r+2} \to h_{2n-2r+4}$, the $n - r + 2$ double roots of the equation $h^2_{n-r+2} = 0$ split into $n - r + 2$ pairs of single roots of $h_{2n-2r+4} = 0$. Thus, the number of loci where hypermultiplets in **15** of $SU(6)$ occur are doubled. A **15** of $SU(6)$ decomposes into **14**$\oplus$**1** (and not **14**′$\oplus$**1**) of $Sp(3)$. Since the adjoint of $SU(6)$ decomposes as **35** = **21**$\oplus$**14**, where **21** is the adjoint of $Sp(3)$, one **14** of $n - r + 2$ hypermultiplets can be thought of as eaten by the $SU(6)$ vector multiplet. Thus, the anomaly-free massless matter spectrum shown in Table 3 can be reproduced if the $n - r + 2 - 1$ hypermultiplets in **14** are "distributed" at the $2n - 2r + 4$ zero loci of $h_{2n-2r+4}$. This, however, seems impossible, since the **14** of $Sp(3)$ is a real representation and does not allow half-hypermultiplets in this representation.

Of course, the original $SU(6)$ spectrum is already anomaly free, so hypermultiplets in **14** cannot be present equally at all the $2n - 2r + 4$ zeros of $h_{2n-2r+4} = 0$ as there are too many to be anomaly free. If they were **14**′ instead of **14**, they could be split into pairs and be equally distributed (up to the eaten ones) at the $2n - 2r + 4$ zeros, but both the heterotic anomaly analysis and Sadov's generalized anomaly cancellation mechanism tell us that they must be **14**, and not **14**′.

This poses the question of how the $n - r + 1$ matter in **14** of $Sp(3)$ are generated and where they reside in the non-split I_6 model. In the next section, in order to explore what happens near a zero locus of $h_{2n-2r+4}$, we perform an explicit blow-up of the singularity.

Downloaded from https://academic.oup.com/ptep/article/2022/3/033B09/6534943 by DESY-Zentralbibliothek user on 25 April 2022

4. Resolutions of the singularities

4.1 *The local equation*

In this section we carry out the process of blow-up of the codimension-two singularity at a zero locus of $h_{2n-2r+4} = 0$. To this end, we consider a local equation in which the enhancement of "A_5" to "D_6" is achieved at codimension two.[8] To obtain such an equation, We first complete the square with respect to y in Eq. (10) and substitute Eq. (12) into it. Writing $y + \frac{1}{2}(a_1 x + a_3) \equiv Y$, we have

$$\begin{aligned} &- Y^2 + x^3 + x^2\left(3t_r^2 h_{n-r+2}^2 - 3z t_r H_{n-r+4}\right) \\ &+ x\left(z^3 t_r f_{n-r+8} + f_8 z^4 + 6z^2 t_r u_{r+4} h_{n-r+2}^2 - 3z^3 u_{r+4} H_{n-r+4}\right) \\ &+ 3z^4 u_{r+4}^2 h_{n-r+2}^2 + z^5 u_{r+4} f_{n-r+8} + g_{12} z^6 = 0, \end{aligned} \tag{16}$$

in which the h_{n-r+2}s appear only in the form h_{n-r+2}^2. Thus, we can make a replacement $h_{n-r+2}^2 \to h_{2n-2r+4}$ in Eq. (16). By setting[9]

$$\begin{aligned} h_{n-r+2}^2 &\to h_{2n-2r+4} = w, \\ t_r = H_{n-r+4} &= u_{r+4} = \frac{1}{\sqrt{3}}, \\ f_{n-r+8} &= f_8 = g_{12} = 0, \end{aligned} \tag{17}$$

we can obtain the desired equation, but it is more convenient to make a shift in the x coordinate: $x + z^2 \equiv X$. In terms of X, the final equation is

$$-Y^2 + X^3 + X^2\left(w - z(3z+1)\right) + X(3z+1)z^3 - z^6 = 0, \tag{18}$$

which we blow up in the following section.

If we write Eq. (18) as

$$-Y^2 + X^3 + \frac{b_2}{4}X^2 + \frac{b_4}{2}X + \frac{b_6}{4} = 0, \tag{19}$$

the vanishing orders of the sections b_2, b_4, and b_6 in z are 0, 3, and 6, respectively, which satisfy the criteria for the I_6-type Kodaira fiber in Tate's algorithm. This is due to the shift $x + z^2 \equiv X$, as without it one would instead have the vanishing orders 0, 2, 4. Note that such a shift of the variable x to eliminate the order-2 term in z from b_4 is not possible globally, since near a zero locus of t_r, where a $\frac{1}{2}\mathbf{20}$ of $SU(6)$ (or $\frac{1}{2}(\mathbf{14}' \oplus \mathbf{6})$ of $Sp(3)$) appears, the necessary shift becomes divergent. This is why an equation with ord$(b_2, b_4, b_6) = (0, 2, 4)$ was used in Refs. [17,18].

4.2 *Blowing up the singularity*

Let us now consider the resolution of the singularity of the local equation in Eq. (18),

$$\Phi(x, y, z, w) \equiv -y^2 + x^3 + x^2\left(w - z(3z+1)\right) + x(3z+1)z^3 - z^6 = 0, \tag{20}$$

where we have replaced X, Y with x, y. Equation (20) has a codimension-one singularity along $(x, y, z) = (0, 0, 0)$ for arbitrary w.

4.2.1 *First blow-up.*

As was done in the previous works, we replace the complex line $(x, y, z) = (0, 0, 0)$ with $\mathbb{P}^2 \times \mathbb{C}$ in $\mathbb{C}^4$ and examine the singularities of the local equations in three

[8] Again, they are quoted because they only imply the Lie algebras whose Dynkin diagrams specify the intersections of the Kodaira fibers right over those points with fixed z'.

[9] In this section, the local coordinates of the base P^1 of F_n (whose affine coordinate is z') will be denoted by w and not by s, in accordance with Ref. [27].

Downloaded from https://academic.oup.com/ptep/article/2022/3/033B09/6534943 by DESY-Zentralbibliothek user on 25 April 2022

different charts corresponding to the affine patches of the $\mathbb{P}^2$ for some fixed w. We also give the explicit forms of the exceptional curves $\mathcal{C}$ at $w \neq 0$ and δs at $w = 0$. (δ is defined by the $w \to 0$ limit of $\mathcal{C}$ in the chart where $\mathcal{C}$ arises.)

Chart 1_x:

$$\begin{aligned}
\Phi(x, xy_1, xz_1, w) &= x^2 \Phi_x(x, y_1, z_1, w), \\
\Phi_x(x, y_1, z_1, w) &= w - x^4 z_1^6 + 3x^3 z_1^4 + x^2(z_1 - 3)z_1^2 - xz_1 + x - y_1^2, \\
\mathcal{C}^{\pm}_{p_1} \text{ in } 1_x &: \ x = 0, \ \ y_1 = \pm\sqrt{w}, \\
\delta_{p_1} \text{ in } 1_x &: \ x = 0, \ \ y_1 = 0, \\
\text{Singularities} &: \ \text{None.}
\end{aligned} \tag{21}$$

Chart 1_y:

$$\begin{aligned}
\Phi(x_1 y, y, yz_1, w) &= y^2 \Phi_y(x_1, y, z_1, w), \\
\Phi_y(x_1, y, z_1, w) &= w x_1^2 + x_1^3 y - x_1^2 y z_1(3yz_1 + 1) + x_1 y^2 z_1^3(3yz_1 + 1) - y^4 z_1^6 - 1, \\
\mathcal{C}^{\pm}_{p_1} \text{ in } 1_y &: \ y = 0, \ \ x_1 = \pm 1/\sqrt{w}, \\
\delta_{p_1} \text{ in } 1_y &: \ \text{Invisible}, \\
\text{Singularities} &: \ \text{None.}
\end{aligned} \tag{22}$$

Chart 1_z:

$$\begin{aligned}
\Phi(x_1 z, y_1 z, z, w) &= z^2 \Phi_z(x_1, y_1, z, w), \\
\Phi_z(x_1, y_1, z, w) &= w x_1^2 + z\left(x_1^3 - x_1^2(3z + 1) + x_1 z(3z + 1) - z^3\right) - y_1^2, \\
\mathcal{C}^{\pm}_{p_1} \text{ in } 1_z &: \ z = 0, \ \ y_1 = \pm\sqrt{w} x_1, \\
\delta_{p_1} \text{ in } 1_z &: \ z = 0, \ \ y_1 = 0, \\
\text{Singularities} &: \ (x_1, y_1, z) = (0, 0, 0).
\end{aligned} \tag{23}$$

Here, chart 1_x is the affine patch of $\mathbb{P}^2 \ni (x : y : z)$ for $x \neq 0$ in which $(x\colon y\colon z) = (1\colon y_1\colon z_1)$. The other charts are similar.[10]

4.2.2 *Second blow-up.* As we can see, the only singularity after the first blow-up is $(x_1, y_1, z) = (0, 0, 0)$ on the chart 1_z, which is not visible from the other charts. This is codimension one, and we blow up this singularity by similarly inserting a one-parameter ($=w$) family of P^2 along $(x_1, y_1, z, w) = (0, 0, 0, w)$. The computation is similar. We find a singularity in the chart 2_{zz}, while the blown-up equations are regular for the charts 2_{zx} and 2_{zy}. Here we show the result for the relavant charts 2_{zx} and 2_{zz}.

[10]Note that we have used the same "z_1" in 1_x and 1_y for different coordinate variables, and similarly for x_1 and y_1. There will be no confusion as we do not compare equations in different charts.

Downloaded from https://academic.oup.com/ptep/article/2022/3/033B09/6534943 by DESY-Zentralbibliothek user on 25 April 2022

Chart 2_{zx}:

$$\begin{aligned}
\Phi_z(x_1, x_1y_2, x_1z_2, w) &= x_1^2\Phi_{zx}(x_1, y_2, z_2, w),\\
\Phi_{zx}(x_1, y_2, z_2, w) &= x_1(z_2-1)z_2 - x_1^2(z_2-1)^3 + w - y_2^2,\\
\mathcal{C}^{\pm}_{p_2} \text{ in } 2_{zx} &: x_1 = 0,\ \ y_2 = \pm\sqrt{w},\\
\delta_{p_2} \text{ in } 2_{zx} &: x_1 = 0,\ \ y_2 = 0,\\
\text{Singularities} &: \text{None.}
\end{aligned} \tag{24}$$

Chart 2_{zz}:

$$\begin{aligned}
\Phi_z(x_2z, y_2z, z, w) &= z^2\Phi_{zz}(x_2, y_2, z, w),\\
\Phi_{zz}(x_2, y_2, z, w) &= wx_2^2 + (x_2-1)z\left(x_2^2z - 2x_2z - x_2 + z\right) - y_2^2,\\
\mathcal{C}^{\pm}_{p_2} \text{ in } 2_{zz} &: z = 0,\ \ y_2 = \pm\sqrt{w}x_2,\\
\delta_{p_2} \text{ in } 2_{zz} &: z = 0,\ \ y_2 = 0,\\
\text{Singularities} &: (x_2, y_2, z) = (0, 0, 0).
\end{aligned} \tag{25}$$

4.2.3 *Third blow-up.* We finally blow up the codimension-one singularity $(x_2, y_2, z) = (0, 0, 0)$ in the chart 2_{zz}. It turns out that this completes the resolution process completely without leaving any singularities.

The equations of the exceptional curve (with a definite w) in the relevant charts are: Chart 3_{zzx}:

$$\begin{aligned}
\Phi_z z(x_2, x_2y_3, x_2z_3, w) &= x_2^2\Phi_{zzx}(x_2, y_3, z_3, w),\\
\Phi_{zzx}(x_2, y_3, z_3, w) &= w + (x_2-1)z_3\left((x_2-1)^2z_3 - 1\right) - y_3^2,\\
\mathcal{C}_{p_3} \text{ in } 3_{zzx} &: x_2 = 0,\ \ y_3^2 = w - (z_3-1)z_3,\\
\delta_{p_3} \text{ in } 3_{zzx} &: x_2 = 0,\ \ y_3^2 = -(z_3-1)z_3,\\
\text{Singularities} &: \text{None.}
\end{aligned} \tag{26}$$

Chart 3_{zzz}:

$$\begin{aligned}
\Phi_z z(x_3z, y_3z, z, w) &= z_2^2\Phi_{zzz}(x_3, y_3, z, w),\\
\Phi_{zzz}(x_3, y_3, z, w) &= x_3^2(w - z(3z+1)) + x_3^3z^3 + 3x_3z + x_3 - y_3^2 - 1 = 0,\\
\mathcal{C}_{p_3} \text{ in } 3_{zzz} &: z_2 = 0,\ \ y_3^2 = wx_3^2 + x_3 - 1,\\
\delta_{p_3} \text{ in } 3_{zzz} &: z_2 = 0,\ \ y_3^2 = x_3 - 1,\\
\text{Singularities} &: \text{None.}
\end{aligned} \tag{27}$$

This completes the blowing-up process, and the space is now smooth. We have seen that conifold singularities do not appear at any stage of the blow-up at the D_6 points. This is similar to the case of the incomplete resolution at the E_6 point in the split I_6 model. However, unlike that case, the intersection of the exceptional curves does not change at all at the D_6 points, as we will see in the next section.

Downloaded from https://academic.oup.com/ptep/article/2022/3/033B09/6534943 by DESY-Zentralbibliothek user on 25 April 2022

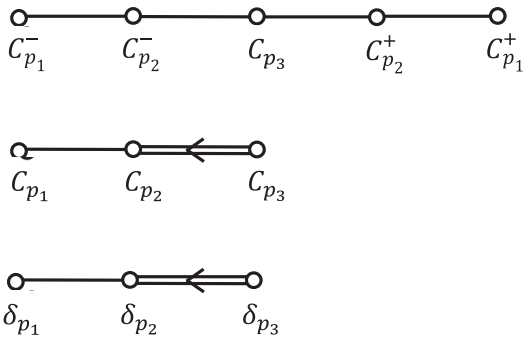

Fig. 1. Intersection diagrams of the exceptional curves. (Top) $w \neq 0$ before the projection in Eq. (28). (Middle) $w \neq 0$ after the projection in Eq. (28). (Bottom) $w = 0$.

4.3 *Intersections of the exceptional curves*

At fixed $w \neq 0$ we have five exceptional curves $\mathcal{C}^{\pm}_{p_1}$, $\mathcal{C}^{\pm}_{p_2}$, and $\mathcal{C}_{p_3}$. From the above explicit forms, one finds that their intersection matrix is given by the A_5 Dynkin diagram (the top diagram of Fig. 1). Although $\mathcal{C}^{\pm}_{p_1}$ and $\mathcal{C}^{\pm}_{p_2}$ are respectively factorized into two lines on this fixed $w \neq 0$ plane, they do not factor in the polynomial ring of w. The two lines at some fixed $w \neq 0$ are interchanged with each other at $w = 0$, meaning that this is a non-split type of singularity. Thus, the two lines for $\mathcal{C}^{\pm}_{p_1}$ or $\mathcal{C}^{\pm}_{p_2}$ at fixed $w \neq 0$ comprising the Kodaira fibers of type I_6 are identified. Hence we define

$$\mathcal{C}_{p_i} \equiv \frac{1}{2}\left(\mathcal{C}^{+}_{p_i} + \mathcal{C}^{-}_{p_i}\right) \qquad (i = 1, 2), \tag{28}$$

which are the projections onto the components invariant under the diagram automorphism of the A_5 Dynkin diagram. Then, one can show that the three exceptional curves $\mathcal{C}_{p_1}$, $\mathcal{C}_{p_2}$, and $\mathcal{C}_{p_3}$ form a non-simply-laced Dynkin diagram of C_3 (the middle diagram of Fig. 1).

At $w = 0$ we again encounter another difference between the present non-split case and the previous examples of singularities associated with the magic square. In the incomplete resolutions for the previous examples $(G, H) = (E_6, SU(6))$, $(E_7, SO(12))$, and (E_8, E_7), while the number of exceptional fibers at $w = 0$ is the same as that at $w \neq 0$, some of the exceptional fibers at $w = 0$ turn out to be linear combinations of those at $w \neq 0$. Therefore, the intersection diagram of the exceptional fibers at $w = 0$ becomes different from that at $w \neq 0$, as summarized in Sect. 2.2. Here, we see something different. As in the previous works, by lifting up the exceptional curves from the defining chart into subsequent charts and seeing their relations, one finds that

$$\mathcal{C}^{\pm}_{p_1} \to \delta_{p_1}, \qquad \mathcal{C}^{\pm}_{p_2} \to \delta_{p_2}, \qquad \mathcal{C}_{p_3} \to \delta_{p_3}. \tag{29}$$

Substituting them into Eq. (28), we obtain

$$\mathcal{C}_{p_1} \to \delta_{p_1}, \qquad \mathcal{C}_{p_2} \to \delta_{p_2}, \qquad \mathcal{C}_{p_3} \to \delta_{p_3}. \tag{30}$$

Thus, the intersection matrix remains identical even at the codimension-two point (see the bottom diagram of Fig. 1). This is in sharp contrast to the previous examples, where the intersection matrices at $w = 0$ did not coincide with any of (the minus of) the Lie algebra Cartan matrices.

Downloaded from https://academic.oup.com/ptep/article/2022/3/033B09/6534943 by DESY-Zentralbibliothek user on 25 April 2022

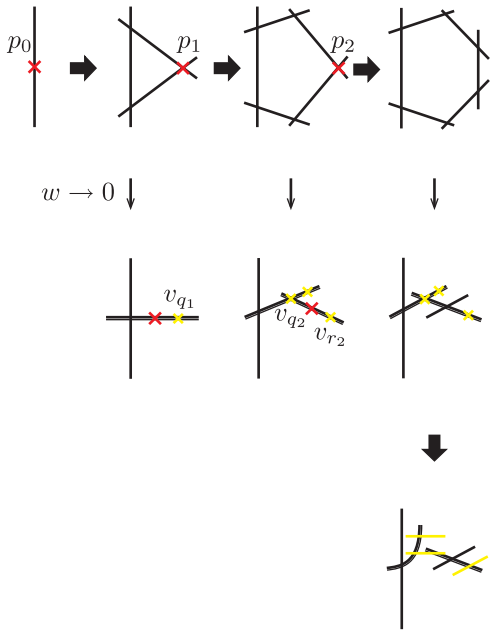

Fig. 2. Resolution of the split I_6 model.

5. Split/non-split transition as a conifold transition

In the previous section we saw that there is no sign of local matter fields near the D_6 points. In this section we use the recent result of Ref. [27] to illustrate how the matter fields are considered to arise near the D_6 points in the non-split I_6 model. In a nutshell, what was found in Ref. [27] is that a transition from the split to the non-split model in F-theory is in most cases a transition from the deformed side to the resolved side in the conifold transition associated with the conifold singularities which arise at D_{2k} points (or E_7 points for the non-split IV^*, which are irrelevant here). In the present case they are D_6 points, so they are precisely what we have been considering in the previous sections.

If we consider the resolution of the split I_6 model instead of the non-split one, we find various conifold singularities (Fig. 2). Indeed, by replacing w with w^2 in Eq. (21), we find

$$\begin{aligned}\Phi_x(x, y_1, z_1, w^2) &= w^2 - x^4 z_1^6 + 3x^3 z_1^4 + x^2(z_1 - 3)z_1^2 - xz_1 + x - y_1^2 \\ &= -y_1^2 + w^2 - x(z_1 + O(x)),\end{aligned} \tag{31}$$

which shows that

$$v_{q_1} : (x, y_1, z_1, w) = (0, 0, 0, 0) \tag{32}$$

is a conifold singularity. Also, in Eq. (24), $\Phi_{zx}(x_1, y_2, z_2, w^2)$ becomes

$$\begin{aligned}\Phi_{zx}(x_1, y_2, z_2, w^2) &= x_1(z_2 - 1)z_2 - x_1^2(z_2 - 1)^3 + w^2 - y_2^2 \\ &= -y_2^2 + w^2 + x_1\left((z_2 - 1)z_2 + O(x_1)\right),\end{aligned} \tag{33}$$

showing that

$$v_{q_2} : (x_1, y_2, z_2, w) = (0, 0, 0, 0) \quad \text{and} \quad v_{r_2} : (x_1, y_2, z_2, w) = (0, 0, 1, 0) \tag{34}$$

are conifold singularities. In this case, it can be shown that the exceptional curves arising from their small resolutions precisely yield (together with the ones coming from the codimension-one singularities) the D_6 Dynkin diagram as their intersection diagram (Fig. 2).

Downloaded from https://academic.oup.com/ptep/article/2022/3/033B09/6534943 by DESY-Zentralbibliothek user on 25 April 2022

In both the split and non-split cases, we can say that the D_6 point is where $h_{2n-2r+4}$ vanishes, and the split case is when $h_{2n-2r+4}$ is in the special form h_{n-r+2}^2. In other words, in the split model a D_6 point is a double root of the equation $h_{2n-2r+4}=0$, whereas in the non-split model it is a single root. So, suppose that $h_{2n-2r+4}=w^2$ near $w=0$ in the split case. Then, by a deformation of the complex structure $w^2 \to w^2-\epsilon^2=(w+\epsilon)(w-\epsilon)$ for some small deformation parameter ϵ, the double zero $w=0$ becomes a pair of single roots $w=\pm\epsilon$, and the split model becomes a non-split model accordingly. On the other hand, as we can see in Eqs. (31) and (33), changing w^2 to $w^2-\epsilon^2$ is exactly turning a conifold into a deformed conifold. Therefore, we see that, at the stage where we have finished blowing up all the codimension-one singularities and only conifold singularities remain, what we get by a small resolution is a split model, and what we get by a deformation is a non-split model. In other words, the split/non-split transition is a conifold transition [27].

Once this fact is revealed, it is not surprising that the conifold singularity does not appear in the non-split model. Since the non-split model corresponds to a deformed conifold, the two-cycles in the split model that are responsible for the matter generation are replaced by three-cycles in the non-split model.

How do these three-cycles give rise to massless matter fields? In Ref. [27] we discussed several possibilities. One is the wrapped M5-branes around $S^2\times S^3$. Since the massless matter in the split model is accounted for by the wrapped M2-branes around the vanishing two-cycles, this would be a natural guess. The total volume of $S^2\times S^3$ will vanish at the apex of the deformed conifold as the volume of S_2 vanishes there. Also, it must contain at least one dimension of the elliptic fiber, for which a small volume limit is taken in the F-theory limit. We cannot say anything conclusive in this paper, so we leave the clarification of the precise mechanism as an issue for the future.

6. Conclusions

Motivated by the coincidence between the three examples of half-hypermultiplets and the entries of the magic square, we have studied a six-dimensional $\mathcal{N}=1$ F-theory compactification on an elliptic fibration over a Hirzebruch surface with a codimension-one singularity of the *non-split* I_6 type found in Ref. [4]. This model supports an $Sp(3)$ gauge symmetry. The heterotic index and generalized Green–Schwarz analysis both show that such a compactification gives massless half-hypermultiplets in the $\mathbf{14}'$ representation (as well as the $\mathbf{6}$ reprentation) of $Sp(3)$, which is $F_4/(Sp(3)\times SU(2))\,(Sp(4)/(Sp(3)\times SU(2)))$. We have shown that they are generated at the E_6 points, where half-hypermultiplets $\mathbf{20}$ of $SU(6)$ would have appeared in the split model. In the non-split model, $SU(6)$ is broken to $Sp(3)$, and $\mathbf{20}$ is decomposed into $\mathbf{14}'\oplus\mathbf{6}$ of $Sp(3)$ accordingly, yielding the desired multiplets.

We have also considered the problem on the non-local matter generation near the D_6 point, and have pointed out two puzzles: The first is how the degrees of massless matter fields in the split model can be plausibly assigned at the zero loci of the relevant section $h_{2n+4-2r}$, the number of which is doubled in the transition from the split to non-split models. Second, by performing a singularity resolution, we found no indication of the existence of localized massless matter fields. We have explained why this is so by using the result of Ref. [27] that the split/non-split transition can be regarded as a conifold transition.

Downloaded from https://academic.oup.com/ptep/article/2022/3/033B09/6534943 by DESY-Zentralbibliothek user on 25 April 2022

Acknowledgment
We thank Y. Kimura and H. Otsuka for useful discussions.

Funding
Open Access funding: SCOAP[3].

References
[1] C. Vafa, Nucl. Phys. B **469**, 403 (1996) [arXiv:hep-th/9602022] [Search inSPIRE].
[2] D. R. Morrison and C. Vafa, Nucl. Phys. B **473**, 74 (1996) [arXiv:hep-th/9602114] [Search inSPIRE].
[3] D. R. Morrison and C. Vafa, Nucl. Phys. B **476**, 437 (1996) [arXiv:hep-th/9603161] [Search inSPIRE].
[4] M. Bershadsky, K. Intriligator, S. Kachru, D. R. Morrison, V. Sadov, and C. Vafa, Nucl. Phys. B **481**, 215 (1996) [arXiv:hep-th/9605200] [Search inSPIRE].
[5] S. H. Katz and C. Vafa, Nucl. Phys. B **497**, 146 (1997) [arXiv:hep-th/9606086] [Search inSPIRE].
[6] T. Tani, Nucl. Phys. B **602**, 434 (2001).
[7] G. Curio, Phys. Lett. B **435**, 39 (1998) [arXiv:hep-th/9803224] [Search inSPIRE].
[8] D. E. Diaconescu and G. Ionesei, J. High Energy Phys. **9812**, 001 (1998) [arXiv:hep-th/9811129] [Search inSPIRE].
[9] S. Mizoguchi and T. Tani, Prog. Theor. Exp. Phys. **2016**, 073B05 (2016) [arXiv:1508.07423 [hep-th]] [Search inSPIRE].
[10] S. Mizoguchi and T. Tani, J. High Energy Phys. **11**, 053 (2016) [arXiv:1607.07280 [hep-th]] [Search inSPIRE].
[11] K. Oguiso and T. Shioda, Comment. Math. Univ. St. Pauli. **40**, 83 (1991).
[12] J. A. Wolf, J. Math. Mech. **14**, 1033 (1965).
[13] D. V. Alekseevskii, Funct. Anal. Appl. **2**, 97 (1968).
[14] D. V. Alekseevskii, Funct. Anal. Appl. **2**, 106 (1968).
[15] D. V. Alekseevskii, Math. USSR Izv. **9**, 297 (1975).
[16] K. Dasgupta, V. Hussin, and A. Wissanji, Nucl. Phys. B **793**, 34 (2008) [arXiv:0708.1023 [hep-th]] [Search inSPIRE].
[17] D. R. Morrison and W. Taylor, J. High Energy Phys. **1201**, 022 (2012) [arXiv:1106.3563 [hep-th]] [Search inSPIRE].
[18] N. Kan, S. Mizoguchi, and T. Tani, arXiv:2003.05563 [hep-th] [Search inSPIRE]
[19] S. Mizoguchi, J. High Energy Phys. **1407**, 018 (2014) [arXiv:1403.7066 [hep-th]] [Search inSPIRE].
[20] T. Kugo and T. Yanagida, Phys. Lett. **134B**, 313 (1984).
[21] A. Grassi, J. Halverson, C. Long, J. L. Shaneson, and J. Tian, J. High Energy Phys. **09**, 129 (2018) [arXiv:1805.06949 [hep-th]] [Search inSPIRE].
[22] P. Arras, A. Grassi, and T. Weigand, J. Geom. Phys. **123**, 71 (2018).
[23] M. Esole, P. Jefferson, and M. J. Kang, [arXiv:1704.08251 [hep-th] [Search inSPIRE]
[24] M. Esole and M. J. Kang, J. High Energy Phys. **02**, 091 (2019) [arXiv:1805.03214 [hep-th]] [Search inSPIRE].
[25] M. Esole and P. Jefferson, arXiv:1910.09536 [hep-th] [Search inSPIRE]
[26] A. Sen, Nucl. Phys. B **475**, 562 (1996) [arXiv:hep-th/9605150] [Search inSPIRE].
[27] R. Kuramochi, S. Mizoguchi, and T. Tani, arXiv:2108.10136 [hep-th] [Search inSPIRE]
[28] M. Gunaydin, G. Sierra, and P. K. Townsend, Phys. Lett. B **133**, 72 (1983).
[29] M. Gunaydin, G. Sierra, and P. K. Townsend, Nucl. Phys. B **242**, 244 (1984).
[30] N. Kan and S. Mizoguchi, Phys. Lett. B **762**, 177 (2016) [arXiv:1605.01904 [hep-th]] [Search inSPIRE].
[31] S. Fukuchi and S. Mizoguchi, Phys. Lett. B **781**, 77 (2018) [arXiv:1802.06555 [hep-th]] [Search inSPIRE].
[32] M. B. Green, J. H. Schwarz, and P. C. West, Nucl. Phys. B **254**, 327 (1985).
[33] N. Yamatsu, arXiv:1511.08771 [hep-ph] [Search inSPIRE].

Downloaded from https://academic.oup.com/ptep/article/2022/3/033B09/6534943 by DESY-Zentralbibliothek user on 25 April 2022

[34] V. Sadov, Phys. Lett. B **388**, 45 (1996) [arXiv:hep-th/9606008] [Search inSPIRE].
[35] H. Hayashi, C. Lawrie, D. R. Morrison, and S. Schafer-Nameki, J. High Energy Phys. **1405**, 048 (2014) [arXiv:1402.2653 [hep-th]] [Search inSPIRE].
[36] S. Mizoguchi and T. Tani, J. High Energy Phys. **03**, 121 (2019) [arXiv:1808.08001 [hep-th]] [Search inSPIRE].

Downloaded from https://academic.oup.com/ptep/article/2022/3/033B09/6534943 by DESY-Zentralbibliothek user on 25 April 2022